

LETTER

Secrecy Outage Probability and Secrecy Diversity Order of Alamouti STBC with Decision Feedback Detection over Time-Selective Fading Channels

Gyulim KIM[†], Nonmember, Hoojin LEE^{††}, Member, Xinrong LI^{†††}, and Seong Ho CHAE^{†††a)}, Nonmembers

SUMMARY This letter studies the secrecy outage probability (SOP) and the secrecy diversity order of Alamouti STBC with decision feedback (DF) detection over the time-selective fading channels. For given temporal correlations, we have derived the exact SOPs and their asymptotic approximations for all possible combinations of detection schemes including joint maximum likelihood (JML), zero-forcing (ZF), and DF at Bob and Eve. We reveal that the SOP is mainly influenced by the detection scheme of the legitimate receiver rather than eavesdropper and the achievable secrecy diversity order converges to two and one for JML only at Bob (i.e., JML-JML/ZF/DF) and for the other cases (i.e., ZF-JML/ZF/DF, DF-JML/ZF/DF), respectively. Here, p - q combination pair indicates that Bob and Eve adopt the detection method $p \in \{\text{JML}, \text{ZF}, \text{DF}\}$ and $q \in \{\text{JML}, \text{ZF}, \text{DF}\}$, respectively.

key words: secrecy outage probability, secrecy diversity order, Alamouti space-time block coding, time-selective fading, decision feedback detection

1. Introduction

The wireless communication is vulnerable to eavesdropping due to the broadcast nature of the radio signals. The security is an important issue in wireless communication and the physical layer security (PLS) has recently drawn much attention as one of the solutions. The PLS ensures secure communication by exploiting the physical characteristics of wireless channel [1]. The first orthogonal space-time block code (STBC) was proposed by Alamouti for two transmit antennas system over the quasi-static channels [2]. There have been several works to study the PLS for Alamouti-STBC based secure communication [3]–[5]. The secrecy outage probabilities (SOPs) of Alamouti-STBC transmission with two transmit antenna selection and power allocation in the absence/presence of feedback errors were studied in the multiple-input multiple-output (MIMO) wiretap channels [3], [4]. The SOP of the quasi-orthogonal STBC which linearly combines two Alamouti STBCs with unequal power scaling was investigated in the MIMO wiretap channels [5].

However, those works were conducted over the quasi-static fading channels, so their results cannot be applicable to the time-selective fading channels.

There have been also some studies for PLS over the time-selective fading channels [6]–[8]. The effects of outdated channel state information were investigated in terms of the SOP in the wiretap channels with transmit antenna selection [6], but it did not consider the Alamouti STBC. In [7], the secrecy transmission rates of Alamouti STBC with zero-forcing (ZF) and joint maximum-likelihood (JML) detections were analyzed over the time-selective fading channel. In [8], the SOP and the secrecy diversity order of Alamouti STBC with ZF and JML detections were studied over time-selective fading channels. However, those works did not consider the efficient decision feedback (DF) detection, so the impacts of DF detection on the secrecy performance have not been studied yet.

Motivated by this, this letter generalizes the results of the previous work [8] by additionally considering the DF detection and investigates how the DF detection affects on the SOP and the secrecy diversity order. Specifically, we consider JML, ZF, and DF as the detection strategies of the legitimate receiver and the eavesdropper and analyze both SOPs and secrecy diversity orders for their all possible combinations. We discover that the SOP is dominantly affected by the detection scheme of Bob rather than Eve and the secrecy diversity order of two and one can be achieved for JML only at Bob (i.e., JML-JML/ZF/DF) and for the other cases (i.e., ZF-JML/ZF/DF, DF-JML/ZF/DF), respectively. Here, p - q combination pair indicates that Bob and Eve adopt the detection method $p \in \{\text{JML}, \text{ZF}, \text{DF}\}$ and $q \in \{\text{JML}, \text{ZF}, \text{DF}\}$, respectively.

2. System Model

We consider the wiretap channels, where a transmitter (Alice) sends the message via Alamouti STBC to a legitimate receiver (Bob) and a passive eavesdropper (Eve) overhears it. Alice has two transmit antennas and Bob and Eve have a single receive antenna. The channels are assumed to experience the time-selective Rayleigh fading. The channels vary for every symbol intervals, but they are temporally correlated with a certain degree. For notational simplicity, we denote Bob and Eve as B and E, respectively.

For a given codeword interval, Alice transmits two con-

Manuscript received August 23, 2023.

Manuscript publicized September 19, 2023.

[†]The author is with Department of IT Semiconductor Convergence Engineering, Tech University of Korea, Siheung, South Korea.

^{††}The author is with the Department of Convergence Security, Hansung University, Seoul, South Korea.

^{†††}The author is with the Department of Electrical Engineering, University of North Texas, Denton, TX, USA.

^{††††}The author is with the Department of Electronics Engineering, Tech University of Korea, Siheung, South Korea.

a) E-mail: shchae@tukorea.ac.kr (Corresponding author)

DOI: 10.1587/transfun.2023EAL2080

secutive data symbols s_1 and s_2 via the Alamouti STBC [2]. Then, the received signal of Bob and Eve (i.e., $k \in \{B, E\}$) over two time instants can be expressed as

$$\underbrace{\begin{bmatrix} r_{k,1} \\ r_{k,2}^* \end{bmatrix}}_{\mathbf{r}_k} = \underbrace{\begin{bmatrix} h_{k,1,1} & h_{k,2,1} \\ h_{k,2,2}^* & -h_{k,1,2}^* \end{bmatrix}}_{\mathbf{H}_k} \underbrace{\begin{bmatrix} s_1 \\ s_2 \end{bmatrix}}_{\mathbf{s}} + \underbrace{\begin{bmatrix} z_{k,1} \\ z_{k,2}^* \end{bmatrix}}_{\mathbf{z}_k}, \quad (1)$$

where $\mathbb{E}[s_1^2] = \mathbb{E}[s_2^2] = E_s$, \mathbf{r}_k and \mathbf{z}_k represent the received signal vector and the additive noise vector of the receiver $k \in \{B, E\}$, respectively. \mathbf{H}_k indicates the 2×2 channel matrix between Alice and the receiver k . $h_{k,i,t}$ represents the channel between the i -th transmit antenna and the receive antenna at the t -th symbol period and is modeled as identically distributed complex Gaussian random variable with zero mean and unit variance. The two time-consecutive channels $h_{k,i,1}$ and $h_{k,i,2}$ are temporally correlated with a correlation degree of $\rho_k \in [0, 1]$, i.e., $\mathbb{E}[h_{k,i,1}h_{k,i,2}^*] = \rho_k$. Note that $\rho_k = 0$ implies the independently time-varying channels, while $\rho_k = 1$ implies the quasi-static channels. $z_{k,t}$ is the additive complex white Gaussian noise with zero mean and variance σ_k^2 at the receiver $k \in \{B, E\}$ at t -th symbol period.

3. Statistics of Three Detection Strategies

When the matched filter matrix is multiplied to the received vector, the decision statistic vector of the receiver $k \in \{B, E\}$ can be obtained as

$$\tilde{\mathbf{r}}_k = \mathbf{G}_k \mathbf{s} + \mathbf{H}_k^H \mathbf{z}_k, \quad (2)$$

where $\mathbf{G}_k = \begin{bmatrix} \varphi_{k,1} & \epsilon_k \\ \epsilon_k^* & \varphi_{k,2} \end{bmatrix}$, $\varphi_{k,1} = |h_{k,1,1}|^2 + |h_{k,2,2}|^2$, $\varphi_{k,2} = |h_{k,1,2}|^2 + |h_{k,2,1}|^2$, $\epsilon_k = h_{k,1,1}^* h_{k,2,1} - h_{k,1,2}^* h_{k,2,2}$. Note that when the channel is quasi-static (i.e., $h_{k,1,1} = h_{k,1,2}$ and $h_{k,2,1} = h_{k,2,2}$), \mathbf{H}_k becomes orthogonal. However, if the channel is time-selective, \mathbf{H}_k becomes non-orthogonal. Thus, ϵ_k in \mathbf{G}_k has a non-zero value which disturbs the decoding of two symbols due to the interference. To eliminate such interference, we consider JML, ZF, and DF detectors.

3.1 Joint Maximum Likelihood (JML) Detection

If the receiver $k \in \{B, E\}$ adopts the joint ML detector, then the pair of symbols (\hat{s}_1, \hat{s}_2) can be detected as follows [8]:

$$\hat{\mathbf{s}}_k^{\text{JML}} = \arg \min_{\mathbf{s} \in \mathcal{S}^2} \|\mathbf{r}_k - \mathbf{H}_k \mathbf{s}\|^2, \quad (3)$$

where \mathcal{S}^2 is the signal constellation. The received SNR for transmit antenna $i = 1, 2$ is given as $\gamma_{k,i}^{\text{JML}} = \frac{E_s}{\sigma_k^2} \varphi_{k,i} = \frac{\bar{\gamma}_k}{2} \varphi_{k,i}$, where $\bar{\gamma}_k = 2E_s/\sigma_k^2$ is the average SNR of the receiver k . The cumulative distribution function (CDF) and probability density function (PDF) of the received SNR at the receiver $k \in \{B, E\}$ are given by

$$F_{\gamma_k^{\text{JML}}}(\gamma) = \mathbb{P}(\gamma_k^{\text{JML}} < \gamma) = 1 - (1 + 2\gamma/\bar{\gamma}_k) e^{-2\gamma/\bar{\gamma}_k}, \quad (4)$$

$$f_{\gamma_k^{\text{JML}}}(\gamma) = \frac{d}{d\gamma} F_{\gamma_k^{\text{JML}}}(\gamma) = (2/\bar{\gamma}_k)^2 \gamma e^{-2\gamma/\bar{\gamma}_k}. \quad (5)$$

3.2 Zero-Forcing (ZF) Detection

The ZF detector is a well-known linear detector which detects every data stream separately by nulling out the interferences coming from other transmit antenna. The symbol detection metric of the ZF detector is expressed as

$$\hat{\mathbf{s}}_k^{\text{ZF}} = \arg \min_{\mathbf{s} \in \mathcal{S}^2} \|r_{k,i}^{\text{ZF}} - \zeta_k \varphi_{k,3-i}^{-1/2} s_i\|^2, \text{ for } i = 1, 2, \quad (6)$$

where $\mathbf{\Phi}_k \mathbf{G}_k^{-1} \mathbf{H}_k^H \mathbf{r}_k = [r_{k,1}^{\text{ZF}}, r_{k,2}^{\text{ZF}}]^T$, $\mathbf{\Phi}_k = \text{diag}(\zeta_k \varphi_{k,2}^{-1/2}, \zeta_k \varphi_{k,1}^{-1/2})$, $\zeta_k = |h_{k,1,1} h_{k,1,2}^* + h_{k,2,1} h_{k,2,2}^*|$. The instantaneous received SNR of the ZF detector for the transmit antenna $i = 1, 2$ is represented by $\gamma_{k,i}^{\text{ZF}} = \frac{\zeta_k^2 E_s}{\varphi_{k,3-i} \sigma_k^2} = \frac{\zeta_k^2}{2\varphi_{k,3-i}} \bar{\gamma}_k$. Since $\gamma_{k,1}^{\text{ZF}}$ and $\gamma_{k,2}^{\text{ZF}}$ have the same statistical distribution, if we represent $\gamma_{k,1}^{\text{ZF}}$ and $\gamma_{k,2}^{\text{ZF}}$ as an unified random variable γ_k^{ZF} , its CDF and PDF can be represented by [8]

$$F_{\gamma_k^{\text{ZF}}}(\gamma) = \mathbb{P}(\gamma_k^{\text{ZF}} < \gamma) = 1 - (1 + 2|\rho_k|^2 \gamma / \bar{\gamma}_k) e^{-2\gamma/\bar{\gamma}_k}, \quad (7)$$

$$f_{\gamma_k^{\text{ZF}}}(\gamma) = (2(1 - |\rho_k|^2) / \bar{\gamma}_k + (2|\rho_k|^2 / \bar{\gamma}_k)^2 \gamma) e^{-2\gamma/\bar{\gamma}_k}. \quad (8)$$

3.3 Decision Feedback (DF) Detection

When the receiver $k \in \{B, E\}$ adopts the DF detector, the decision metric can be expressed as [9]

$$\hat{s}_{k,1} = \arg \min_{s \in \mathcal{S}} \left\| r_{k,1} - (\zeta_k / \sqrt{\varphi_{k,2}}) s \right\|^2, \quad (9)$$

$$\hat{s}_{k,2} = \arg \min_{s \in \mathcal{S}} \left\| r_{k,2} - \sqrt{\varphi_{k,2}} s - (\epsilon_k^* / \sqrt{\varphi_{k,2}}) \hat{s}_{k,1} \right\|^2. \quad (10)$$

As in the DF analysis [9], the SNRs of the DF detector can be assumed as $\gamma_1^{\text{DF}} = \gamma_1^{\text{ZF}}$ and $\gamma_2^{\text{DF}} = \gamma_2^{\text{JML}}$. Thus, the CDF and PDF of the receiver k can be approximated as

$$F_{\gamma_k^{\text{DF}}}(\gamma) \simeq \frac{1}{2} (F_{\gamma_k^{\text{ZF}}}(\gamma) + F_{\gamma_k^{\text{JML}}}(\gamma)) \quad (11)$$

$$= 1 - \left(1 + (1 + |\rho_k|^2) \gamma / \bar{\gamma}_k\right) e^{-2\gamma/\bar{\gamma}_k}, \quad (12)$$

$$f_{\gamma_k^{\text{DF}}}(\gamma) \simeq (2\gamma(1 + |\rho_k|^2) / \bar{\gamma}_k^2 + (1 - |\rho_k|^2) / \bar{\gamma}_k) e^{-2\gamma/\bar{\gamma}_k}. \quad (13)$$

4. Analysis of Secrecy Outage Probability and Secrecy Diversity Order

In this section, we analyze the SOP of Alamouti STBC for the combinations of three different detection techniques such as JML, ZF, and DF over the time-selective fading channels.

When Bob and Eve adopt the detection techniques $p \in \{\text{JML}, \text{ZF}, \text{DF}\}$ and $q \in \{\text{JML}, \text{ZF}, \text{DF}\}$, respectively, the secrecy capacity which is defined as the maximum achievable rate for the desired receiver while preventing Eve from obtaining any useful information is expressed as

$$C_s^{p,q} = \left[C_B^p - C_E^q \right]^+, \quad (14)$$

Table 1 The SOPs for all possible combinations of JML, ZF, and DF detectors at Bob and Eve.

| Bob (p) | Eve (q) | $P_{\text{so}}^{p,q}(R_s)$ |
|-------------|-------------|---|
| JML | JML | $P_{\text{so}}^{\text{JML,JML}}(R_s) = \int_0^\infty \left(\frac{2}{\bar{\gamma}_E}\right)^2 \gamma_E e^{-\frac{2}{\bar{\gamma}_E} \gamma_E} \left[1 - \left(1 + \frac{2}{\bar{\gamma}_B} (2^{R_s} (1 + \gamma_E) - 1)\right) e^{-\frac{2}{\bar{\gamma}_B} (2^{R_s} (1 + \gamma_E) - 1)}\right] d\gamma_E$ |
| JML | ZF | $P_{\text{so}}^{\text{JML,ZF}}(R_s) = \int_0^\infty \left(\frac{2(1- \rho_E ^2)}{\bar{\gamma}_E} + \left(\frac{2 \rho_E ^2}{\bar{\gamma}_E}\right)^2 \gamma_E\right) e^{-\frac{2}{\bar{\gamma}_E} \gamma_E} \left[1 - \left(1 + \frac{2}{\bar{\gamma}_B} (2^{R_s} (1 + \gamma_E) - 1)\right) e^{-\frac{2}{\bar{\gamma}_B} (2^{R_s} (1 + \gamma_E) - 1)}\right] d\gamma_E$ |
| JML | DF | $P_{\text{so}}^{\text{JML,DF}}(R_s) = \int_0^\infty \left(\frac{2(1+ \rho_E ^2)}{\bar{\gamma}_E} \gamma + \frac{1- \rho_E ^2}{\bar{\gamma}_E}\right) e^{-\frac{2}{\bar{\gamma}_E} \gamma} \cdot \left[1 - \left(1 + \frac{2}{\bar{\gamma}_B} (2^{R_s} (1 + \gamma_E) - 1)\right) e^{-\frac{2}{\bar{\gamma}_B} (2^{R_s} (1 + \gamma_E) - 1)}\right] d\gamma_E$ |
| ZF | JML | $P_{\text{so}}^{\text{ZF,JML}}(R_s) = \int_0^\infty \left(\frac{2}{\bar{\gamma}_E}\right)^2 \gamma_E e^{-\frac{2}{\bar{\gamma}_E} \gamma_E} \left[1 - \left(1 + \frac{2 \rho_B ^2}{\bar{\gamma}_B} (2^{R_s} (1 + \gamma_E) - 1)\right) e^{-\frac{2}{\bar{\gamma}_B} (2^{R_s} (1 + \gamma_E) - 1)}\right] d\gamma_E$ |
| ZF | ZF | $P_{\text{so}}^{\text{ZF,ZF}}(R_s) = \int_0^\infty \left(\frac{2(1- \rho_E ^2)}{\bar{\gamma}_E} + \left(\frac{2 \rho_E ^2}{\bar{\gamma}_E}\right)^2 \gamma_E\right) e^{-\frac{2}{\bar{\gamma}_E} \gamma_E} \left[1 - \left(1 + \frac{2 \rho_B ^2}{\bar{\gamma}_B} (2^{R_s} (1 + \gamma_E) - 1)\right) e^{-\frac{2}{\bar{\gamma}_B} (2^{R_s} (1 + \gamma_E) - 1)}\right] d\gamma_E$ |
| ZF | DF | $P_{\text{so}}^{\text{ZF,DF}}(R_s) = \int_0^\infty \left(\frac{2(1+ \rho_E ^2)}{\bar{\gamma}_E} \gamma_E + \frac{1- \rho_E ^2}{\bar{\gamma}_E}\right) e^{-\frac{2}{\bar{\gamma}_E} \gamma_E} \cdot \left[1 - \left(1 + \frac{2 \rho_B ^2}{\bar{\gamma}_B} (2^{R_s} (1 + \gamma_E) - 1)\right) e^{-\frac{2}{\bar{\gamma}_B} (2^{R_s} (1 + \gamma_E) - 1)}\right] d\gamma_E$ |
| DF | JML | $P_{\text{so}}^{\text{DF,JML}}(R_s) = \int_0^\infty \left(\frac{2}{\bar{\gamma}_E}\right)^2 \gamma_E e^{-\frac{2}{\bar{\gamma}_E} \gamma_E} \cdot \left[1 - \left(1 + \frac{(1+ \rho_B ^2)}{\bar{\gamma}_B} (2^{R_s} (1 + \gamma_E) - 1)\right) e^{-\frac{2}{\bar{\gamma}_B} (2^{R_s} (1 + \gamma_E) - 1)}\right] d\gamma_E$ |
| DF | ZF | $P_{\text{so}}^{\text{DF,ZF}}(R_s) = \int_0^\infty \left(\frac{2(1- \rho_E ^2)}{\bar{\gamma}_E} + \left(\frac{2 \rho_E ^2}{\bar{\gamma}_E}\right)^2 \gamma_E\right) e^{-\frac{2}{\bar{\gamma}_E} \gamma_E} \cdot \left[1 - \left(1 + \frac{(1+ \rho_B ^2)}{\bar{\gamma}_B} (2^{R_s} (1 + \gamma_E) - 1)\right) e^{-\frac{2}{\bar{\gamma}_B} (2^{R_s} (1 + \gamma_E) - 1)}\right] d\gamma_E$ |
| DF | DF | $P_{\text{so}}^{\text{DF,DF}}(R_s) = \int_0^\infty \left(\frac{2(1+ \rho_E ^2)}{\bar{\gamma}_E} \gamma_E + \frac{1- \rho_E ^2}{\bar{\gamma}_E}\right) e^{-\frac{2}{\bar{\gamma}_E} \gamma_E} \cdot \left[1 - \left(1 + \frac{(1+ \rho_B ^2)}{\bar{\gamma}_B} (2^{R_s} (1 + \gamma_E) - 1)\right) e^{-\frac{2}{\bar{\gamma}_B} (2^{R_s} (1 + \gamma_E) - 1)}\right] d\gamma_E$ |

where $[x]^+ \triangleq \max(x, 0)$ and $C_B^p = \frac{1}{2} \sum_{i=1}^2 \log_2(1 + \gamma_{B,i}^p)$ and $C_E^q = \frac{1}{2} \sum_{i=1}^2 \log_2(1 + \gamma_{E,i}^q)$ represent the channel capacities of Alice-Bob and Alice-Eve links. Then, the SOP can be expressed as [4], [5]

$$P_{\text{so}}^{p,q}(R_s) = \mathbb{P}[C_s^{p,q} < R_s], \quad (15)$$

where R_s is a target secrecy rate. Since the received SNRs of both JML and ZF detectors have the same statistics for all transmit antennas and the received SNR of DF detector is assumed to have the same statistics for all transmit antennas, the received SNRs for all transmit antennas can be represented as the unified random variable as $\gamma_{k,1}^a = \gamma_{k,2}^a \triangleq \gamma_k^a$, where $(k, a) \in \{(B, p), (E, q)\}$. Accordingly, the SOP can be represented by

$$P_{\text{so}}^{p,q}(R_s) = \int_0^\infty f_{\gamma_E^q}(\gamma_E) F_{\gamma_B^p}(2^{R_s}(1 + \gamma_E) - 1) d\gamma_E. \quad (16)$$

By plugging (4), (5), (7), (8), (12), and (13) into (16), we can obtain the SOPs for all possible combinations of JML, ZF, and DF at Bob and Eve. The obtained results are summarized in Table 1. Note that we obtain the new results for SOP for the cases of JML-DF, ZF-DF, DF-DF, DF-JML, DF-ZF compared to the previous work [8].

The secrecy diversity order which characterizes the reliability of secured wireless communication system is defined as the asymptotic ratio of the logarithmic SOP to the logarithmic average SNR of Bob [8], [10]:

$$d^{p,q} = - \lim_{\bar{\gamma}_B \rightarrow \infty} \log P_{\text{so}}^{p,q}(R_s) / \log \bar{\gamma}_B. \quad (17)$$

Note that the diversity order indicates the magnitude of the slope of SOP versus SNR $\bar{\gamma}_B$ on a log-log scale in the high SNR region.

However, since the SOP in Table 1 has an intractable

form with an integral, understanding the asymptotic behavior of SOP with the closed-form expression is difficult. To obtain some useful insights with closed-form expression, we derive the lowerbound of SOP as follows [11], [12]:

$$P_{\text{so}}^{p,q}(R_s) \geq P_{\text{so}}^{p,q,\text{LB}}(R_s) \triangleq \int_0^\infty f_{\gamma_E^q}(\gamma_E) F_{\gamma_B^p}(2^{R_s} \gamma_E) d\gamma_E. \quad (18)$$

Note that the lowerbound becomes tighter as R_s becomes smaller. The lowerbound of the secrecy outage probability is derived from the fact that the CDF of $F_{\gamma_B^p}(2^{R_s}(1 + \gamma_E) - 1)$ in (16) is lower-bounded by $F_{\gamma_B^p}(2^{R_s} \gamma_E)$. Since $2^{R_s}(1 + \gamma_E) - 1 \rightarrow 2^{R_s} \gamma_E$ holds for small R_s , the tightness of both CDFs can hold for small R_s . For high $\bar{\gamma}_B$, the CDFs for the received SNRs of Bob for JML, ZF, DF detections can be simplified by using Taylor series expansion as $F_{\gamma_B^{\text{JML}}}(\gamma) \approx 2(\gamma/\bar{\gamma}_B)^2$, $F_{\gamma_B^{\text{ZF}}}(\gamma) \approx 2(1 - |\rho_B|^2)\gamma/\bar{\gamma}_B$, $F_{\gamma_B^{\text{DF}}}(\gamma) \approx (1 - |\rho_B|^2)\gamma/\bar{\gamma}_B$. By applying these approximated CDFs to (18), we obtain the closed-form expression for SOP as given in Table 2. Using them, the achievable secrecy diversity order can be obtained as given in Table 2.

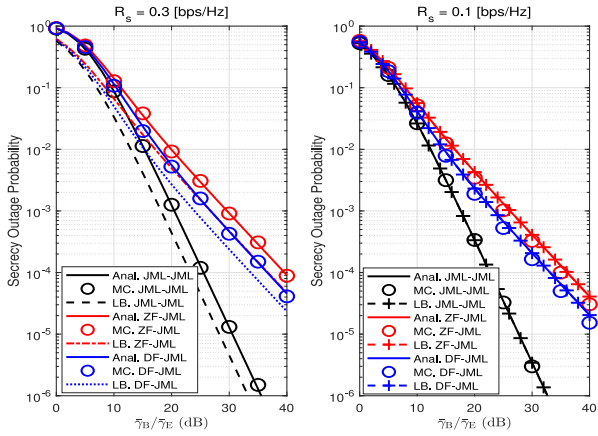
5. Numerical Results

In this section, we evaluate the SOPs of Alamouti STBC over the time-selective Rayleigh fading channels and verify our analytical results. Unless otherwise stated, the simulation environmental settings are as follows: $E_s = 40$ [dBm], $R_s = 0.1$ [bps/Hz], $\rho_B = 0.9$, and $\rho_E = 0.8$.

Figure 1 plots our analytical results for the exact SOPs (Anal.), i.e., Table 1, their lowerbounds (LB.) in (18), and the Monte-Carlo simulation results (MC.) versus the ratio of average SNRs between Bob and Eve, $\bar{\gamma}_B/\bar{\gamma}_E$ for various R_s . The exact SOP and its lowerbound are considerably tight when $R_s = 0.1$ [bps/Hz], while there exists some gaps when $R_s = 0.3$ [bps/Hz]. Although there exists some gaps

Table 2 The asymptotic analysis of the lowerbounded SOPs in high $\bar{\gamma}_B$.

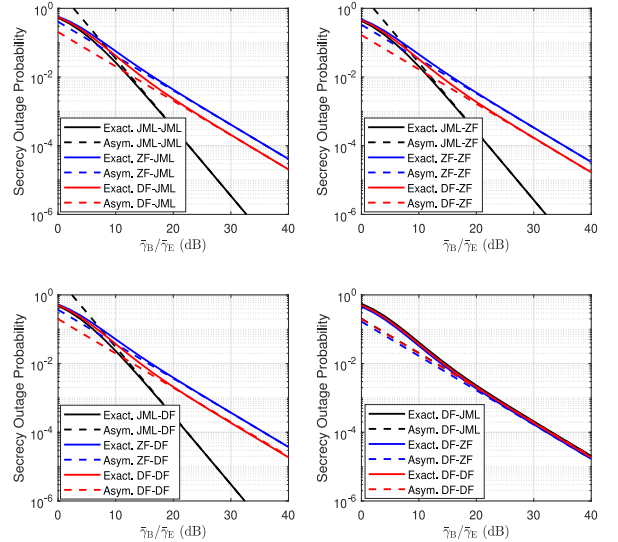
| Bob (p) | Eve (q) | $P_{so, \bar{\gamma}_B \rightarrow \infty}^{p,q, LB}(R_s)$ | $d^{p,q}$ |
|-------------|-------------|---|--|
| JML | JML | $P_{so, \bar{\gamma}_B \rightarrow \infty}^{JML, JML, LB}(R_s) \simeq 3 \cdot 2^{2R_s} \left(\frac{\bar{\gamma}_E}{\bar{\gamma}_B}\right)^2$ | $d^{JML, JML} = -\lim_{\bar{\gamma}_B \rightarrow \infty} \frac{\log(3 \cdot 2^{2R_s} (\bar{\gamma}_E/\bar{\gamma}_B)^2)}{\log \bar{\gamma}_B} \simeq 2$ |
| JML | ZF | $P_{so, \bar{\gamma}_B \rightarrow \infty}^{JML, ZF, LB}(R_s) \simeq 2^{2R_s} (1 + 2 \rho_E ^2) \left(\frac{\bar{\gamma}_E}{\bar{\gamma}_B}\right)^2$ | $d^{JML, ZF} = -\lim_{\bar{\gamma}_B \rightarrow \infty} \frac{\log(2^{2R_s} (1 + 2 \rho_E ^2) (\bar{\gamma}_E/\bar{\gamma}_B)^2)}{\log \bar{\gamma}_B} \simeq 2$ |
| JML | DF | $P_{so, \bar{\gamma}_B \rightarrow \infty}^{JML, DF, LB}(R_s) \simeq 2^{2R_s} (2 + \rho_E ^2) \left(\frac{\bar{\gamma}_E}{\bar{\gamma}_B}\right)^2$ | $d^{JML, DF} = -\lim_{\bar{\gamma}_B \rightarrow \infty} \frac{\log(2^{2R_s} (2 + \rho_E ^2) (\bar{\gamma}_E/\bar{\gamma}_B)^2)}{\log \bar{\gamma}_B} \simeq 2$ |
| ZF | JML | $P_{so, \bar{\gamma}_B \rightarrow \infty}^{ZF, JML, LB}(R_s) \simeq 2^{R_s+1} (1 - \rho_B ^2) \frac{\bar{\gamma}_E}{\bar{\gamma}_B}$ | $d^{ZF, JML} = -\lim_{\bar{\gamma}_B \rightarrow \infty} \frac{\log(2^{R_s+1} (1 - \rho_B ^2) (\bar{\gamma}_E/\bar{\gamma}_B))}{\log \bar{\gamma}_B} \simeq 1$ |
| ZF | ZF | $P_{so, \bar{\gamma}_B \rightarrow \infty}^{ZF, ZF, LB}(R_s) \simeq 2^{R_s} (1 - \rho_B ^2) (1 + \rho_E ^2) \frac{\bar{\gamma}_E}{\bar{\gamma}_B}$ | $d^{ZF, ZF} = -\lim_{\bar{\gamma}_B \rightarrow \infty} \frac{\log(2^{R_s} (1 - \rho_B ^2) (1 + \rho_E ^2) (\bar{\gamma}_E/\bar{\gamma}_B))}{\log \bar{\gamma}_B} \simeq 1$ |
| ZF | DF | $P_{so, \bar{\gamma}_B \rightarrow \infty}^{ZF, DF, LB}(R_s) \simeq 2^{R_s-1} (1 - \rho_B ^2) (3 + \rho_E ^2) \frac{\bar{\gamma}_E}{\bar{\gamma}_B}$ | $d^{ZF, DF} = -\lim_{\bar{\gamma}_B \rightarrow \infty} \frac{\log(2^{R_s-1} (1 - \rho_B ^2) (3 + \rho_E ^2) (\bar{\gamma}_E/\bar{\gamma}_B))}{\log \bar{\gamma}_B} \simeq 1$ |
| DF | JML | $P_{so, \bar{\gamma}_B \rightarrow \infty}^{DF, JML, LB}(R_s) \simeq 2^{R_s} (1 - \rho_B ^2) \frac{\bar{\gamma}_E}{\bar{\gamma}_B}$ | $d^{DF, JML} = -\lim_{\bar{\gamma}_B \rightarrow \infty} \frac{\log(2^{R_s} (1 - \rho_B ^2) (\bar{\gamma}_E/\bar{\gamma}_B))}{\log \bar{\gamma}_B} \simeq 1$ |
| DF | ZF | $P_{so, \bar{\gamma}_B \rightarrow \infty}^{DF, ZF, LB}(R_s) \simeq 2^{R_s-1} (1 - \rho_B ^2) (1 + \rho_E ^2) \frac{\bar{\gamma}_E}{\bar{\gamma}_B}$ | $d^{DF, ZF} = -\lim_{\bar{\gamma}_B \rightarrow \infty} \frac{\log(2^{R_s-1} (1 - \rho_B ^2) (1 + \rho_E ^2) (\bar{\gamma}_E/\bar{\gamma}_B))}{\log \bar{\gamma}_B} \simeq 1$ |
| DF | DF | $P_{so, \bar{\gamma}_B \rightarrow \infty}^{DF, DF, LB}(R_s) \simeq 2^{2R_s-2} (1 - \rho_B ^2) (3 + \rho_E ^2) \frac{\bar{\gamma}_E}{\bar{\gamma}_B}$ | $d^{DF, DF} = -\lim_{\bar{\gamma}_B \rightarrow \infty} \frac{\log(2^{2R_s-2} (1 - \rho_B ^2) (3 + \rho_E ^2) (\bar{\gamma}_E/\bar{\gamma}_B))}{\log \bar{\gamma}_B} \simeq 1$ |

**Fig. 1** Comparison of the exact SOPs, their lowerbounds, and the Monte-Carlo simulation results versus $\bar{\gamma}_B/\bar{\gamma}_E$ for R_s [bps/Hz].

for relatively large R_s , the slopes in high $\bar{\gamma}_B/\bar{\gamma}_E$ between the exact SOP and its lowerbound are the same. This figure validates that the tightness of the lowerbound holds for relatively small R_s , which justifies our analysis for secrecy diversity order from the lowerbounded SOP.

Figure 2 compares the exact SOPs and their asymptotic analytical results, i.e., Table 2, for all possible combinations of JML, ZF, and DF detection methods versus $\bar{\gamma}_B/\bar{\gamma}_E$. This figure shows that the exact SOPs and their asymptotic analysis are perfectly matched in high $\bar{\gamma}_B/\bar{\gamma}_E$, which verifies the accuracy of our analytical results in Table 2. This figure also shows that the SOPs are superior in the order of DF-ZF, DF-DF, and DF-JML and in the order of JML-DF, DF-DF, and ZF-DF for given ρ_B and ρ_E . This implies that the detection strategy is superior in the order of JML, DF, and ZF in terms of signal-to-noise ratio. Moreover, the SOP is dominantly affected by the detection scheme of Bob rather than that of Eve.

Figure 3 compares the instantaneous secrecy diver-

**Fig. 2** Comparison between the exact SOPs and their asymptotic analysis in Table 2.

sity orders of the exact SOP in Table 1 and the asymptotic lowerbounded SOP in Table 2 versus $\bar{\gamma}_B$. The *instantaneous* secrecy diversity order is defined as $\hat{d}^{p,q} = -\log P_{so}^{p,q}(R_s)/\log \bar{\gamma}_B$, where $d^{p,q} = \lim_{\bar{\gamma}_B \rightarrow \infty} \hat{d}^{p,q}$. We can see the similar plots of the instantaneous diversity orders for the SOP (or BER, SER, etc) versus SNR in [13] and [14]. As $\bar{\gamma}_B$ increases, the instantaneous secrecy diversity order of the exact SOP converges to that of the asymptotic lowerbounded SOP, which validates the accuracy of our asymptotic analysis in Table 2. As $\bar{\gamma}_B$ increases, regardless of the detection method of Eve, the instantaneous secrecy diversity order converges to two when Alice adopts JML detection method, while it converges to one when Alice adopts ZF and DF detection methods. This results is perfectly matched to our analysis for asymptotic secrecy diversity order given in Table 2.

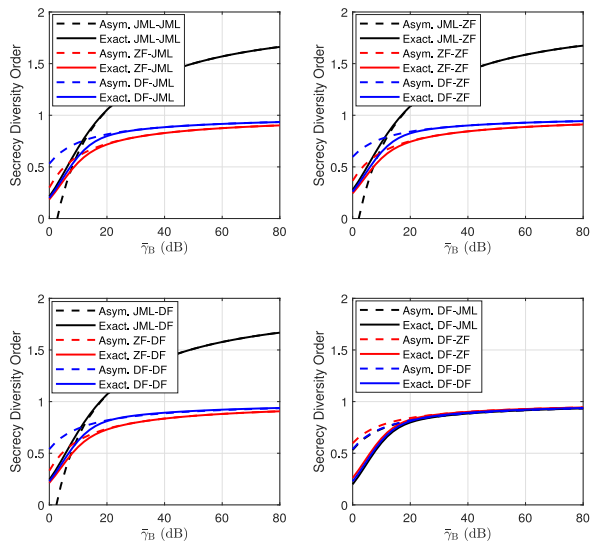


Fig. 3 Comparison of instantaneous secrecy diversity orders of the exact SOP in Table 1 and its asymptotic analysis in Table 2.

6. Conclusion

This letter has studied the SOP and secrecy diversity order of Alamouti STBC especially with DF detection over the time-selective fading channels. For given temporal correlations, we have derived the exact SOPs and their asymptotically high SNR approximation for all possible combinations of detection schemes, i.e., JML, ZF, and DF, at Bob and Eve. We have revealed that the SOP is mainly affected by the detection scheme of the legitimate receiver rather than eavesdropper and the secrecy diversity order converges to two and one for JML only at Bob (i.e., JML-JML/ZF/DF) and for the other cases (i.e., ZF-JML/ZF/DF, DF-JML/ZF/DF), respectively.

Acknowledgments

This research was supported by the National Research Foundation of Korea (NRF) grant funded by the Korea government (MSIT) (No. NRF-2021R1F1A1050633). The work of Hoojin Lee was supported by Hansung University.

References

[1] S.H. Chae, W. Choi, J.H. Lee, and T.Q.S. Quek, "Enhanced secrecy in stochastic wireless networks: Artificial noise with secrecy protected zone," *IEEE Trans. Inf. Forensics Security*, vol.9, no.10, pp.1617–1628, Oct. 2014.

[2] S.M. Alamouti, "A simple transmit diversity technique for wireless communications," *IEEE J. Sel. Areas Commun.*, vol.16, no.8, pp.1451–1458, Oct. 1998.

[3] S. Yan, N. Yang, E. Malaney, and J. Yuan, "Transmit antenna selection with Alamouti coding and power allocation in MIMO wiretap channels," *IEEE Trans. Wireless Commun.*, vol.13, no.3, pp.1656–1667, March 2014.

[4] A.F. Coşkun and O. Kucur, "Secrecy outage probability of conventional and modified TAS/Alamouti-STBC schemes with power allocation in the presence of feedback errors," *IEEE Trans. Veh. Technol.*, vol.68, no.3, pp.2609–2623, March 2019.

[5] S.H. Chae, I. Bang, and H. Lee, "Physical layer security of QSTBC with power scaling in MIMO wiretap channels," *IEEE Trans. Veh. Technol.*, vol.69, no.5, pp.5647–5651, May 2020.

[6] N.S. Ferdinand, D.B. da Costa, and M. Latva-aho, "Effects of outdated CSI on the secrecy performance of MISO wiretap channels with transmit antenna selection," *IEEE Commun. Lett.*, vol.17, no.5, pp.864–867, May 2013.

[7] D. Kim, G. Kim, H. Lee, and S.H. Chae, "On the achievable secrecy transmission rates by Alamouti space-time block coding in time-selective fading channels," *Electronics Letters*, vol.58, no.17, pp.672–674, Aug. 2022.

[8] S.H. Chae and H. Lee, "Secrecy outage probability and diversity order of Alamouti STBC over time-selective fading channels," *ICT Express*, vol.9, no.4, pp.714–721, 2023.

[9] H. Lee, R.W. Heath, and E.J. Powers, "Information outage probability and diversity order of alamouti transmit diversity in time-selective fading channels," *IEEE Trans. Veh. Technol.*, vol.57, no.6, pp.3890–3895, Nov. 2008.

[10] M. Craiti, A. Gharayeb, C. Assi, and M.O. Hasna, "On the achievable secrecy diversity of cooperative networks with untrusted relays," *IEEE Trans. Commun.*, vol.66, no.1, pp.39–53, Jan. 2018.

[11] N. Bhargava, S.L. Cotton, and D.E. Simmons, "Secrecy capacity analysis over κ - μ fading channels: Theory and applications," *IEEE Trans. Commun.*, vol.64, no.7, pp.3011–3024, July 2016.

[12] J. Moualeu, D. Costa, F. Martinez, W. Hamouda, T. Ngatched, and U. Dias, "Transmit antenna selection in secure MIMO systems over α - μ fading channels," *IEEE Trans. Commun.*, vol.67, no.9, pp.6483–6498, Sept. 2019.

[13] H. Lee, J.G. Andrews, and E.J. Powers, "Information outage probability and diversity order of symmetric coordinate interleaved orthogonal designs," *IEEE Trans. Wireless Commun.*, vol.7, no.5, pp.1501–1506, May 2008.

[14] H. Lee, J.G. Andrews, R.W. Heath, and E.J. Powers, "The performance of space-time block codes from coordinate interleaved orthogonal designs over Nakagami-m fading channels," *IEEE Trans. Commun.*, vol.57, no.3, pp.653–664, March 2009.